Supplementary Materials for

Defect-free-induced Na^+ disordering in electrode materials

Jian Peng,[a,b] ‡ Mingyang Ou,[a,] ‡ Haocong Yi,[a,] ‡ Xueping Sun,[a,] ‡ Yuanpeng Zhang,[c,] ‡ Bao Zhang,[d] Yu Ding,[e] Feng Wang, [e] Songqi Gu,[f] Carlos Alberto López,[g] Wang Zhang,[a] Yi Liu,[a] Ju Fang,[h] Peng Wei,[a] Yuyu Li,[a] Ling Miao,[d] Jianjun Jiang,[d] Chun Fang,[a] Qing Li,[a] María Teresa Fernández-Díaz,[i] José Antonio Alonso,[j] Shulei Chou,[b] and Jiantao Han[a,*]

a State Key Laboratory of Material Processing and Die & Mould Technology, School of Materials Science and Engineering, Huazhong University of Science and Technology, Wuhan 430074, P. R. China

b Institute for Superconducting and Electronic Materials, Australian Institute for Innovative Materials, University of Wollongong, Innovation Campus, Squires Way, North Wollongong, NSW 2522, Australia

c Neutron Science Division, Oak Ridge National Laboratory (ORNL), 1 Bethel Valley Rd, Oak Ridge, Tennessee 37831, United States

d School of Optical and Electronic Information, Huazhong University of Science and Technology, Wuhan 430074, P. R. China

e College of Chemistry and Materials Science, Hubei Engineering University, Xiaogan 432000, P. R. China

f Shanghai Synchrotron Radiation Facility, Shanghai Institute of Applied Physics, Chinese Academy of Science, Shanghai, 201204, P. R. China

g Instituto de Investigaciones en Tecnología Química (INTEQUI), UNSL, CONICET and Facultad de Quím., Bioquím. y Farm., UNSL, San Luis, 5700, Argentina.

h Key Laboratory of Artificial Micro- and Nano-structures of Ministry of Education, School of Physics and Technology, Wuhan University, Wuhan 430072, China

i Institut Laue Langevin, F-38042 Grenoble, France.

j Department of Energy&Environment, Instituto de Ciencia de Materiales de Madrid, CSIC, Cantoblanco, E-28049 Madrid, Spain

‡These authors contributed equally to this work.

*E-mail: jthan@hust.edu.cn

Methods

Synthesis of CP-NiHCF. Co-precipitated NiHCF was synthesized by simultaneous dropwise addition of 50 ml of 0.1 M $NiCl_2$ and 50 ml of 0.1 M $Na_4Fe(CN)_6$ to 100 ml of H_2O dropwise under constant stirring for 5 h and then aged for 24 h at room temperature. The green product was then washed thoroughly with DI water and ethanol. Finally, the formed precipitate was dried at 100 °C in a vacuum for 24 h. The sample was marked as material CP-NiHCF.

Synthesis of HQ-NiHCF. HQ-NiHCF was synthesized via a modified coprecipitation method. Typically, 50 ml of 0.1 M $Na_4Fe(CN)_6$ solution and 50 ml of mixed solution with 0.1 M $NiCl_2$, 0.5 M trisodium citrate, 10 g NaCl, and 1.0 g PVP followed by the same method to collect the final product and marked as HQ–NiHCF.

Synthesis of SC−NiHCF. As illustrated in supplementary Fig. 1, secondary crystallization is a process in which the HQ–NiHCF is used as a precursor. After being aged for 24 h, the sample was stirred well and then transferred into reactors. Next, the material was heated to 120°C and maintained for 24 h. Finally, the precipitate in the naturally cooled solution was collected, washed, and dried by the same procedures as above obtain SC-NiHCF. The obtained nickel and cobalt-based PBAs are shown in supplementary Fig. 2.

Synthesis of $NaTi_2(PO_4)_3$ (NTP). 3 g TiO_2, 3 g NaH_2PO_4, 3 mL H_3PO_4 (85 wt% solution), and 3 mL DI water were ground and mixed then transferred into reactors and then heated at 150°C for 6 h. The products were then washed and centrifuged with DI

water several times. For the carbon coating, the prepared $NaTi_2(PO_4)_3$ was mixed with acetone containing 10 wt% glucose. Finally, the solution was dried to obtain a powder that was finally heated at 600°C under argon gas flow in a tube furnace for 4 hours.

Materials characterization. The XRD patterns were obtained using Panalytical X'pert PRO MRD (Holland) with Cu K〈 radiation. The particle size and morphology of products were characterized by FE-SEM (JSM 7600F, JEOL, Japan) and TEM (JEM-2100). LabRAM HR800 (Horiba JobinYvon) Raman spectra were measured by using an Ar ion laser at 532 nm. ICP-OES (IRIS Intrepid II XSP, Thermo Elemental, USA) was used to determine elemental compositions. Thermogravimetry analysis (Netzsch STA 449F3 analyzer) was conducted from ~25 °C to 400 °C with heating rate of 10 °C/min in air.

Structural characterization. Neutron powder diffraction (NPD) experiments were carried out at the ILL, Grenoble, France, in the high-resolution powder diffractometer D2B (λ = 1.594 Å) at room temperature. Here, 2 g of a sample of nominal composition $Na_{1.67}Ni[Fe(CN)_6]_{0.87}\cdot zH_2O$ was placed in a vanadium can for 2 h of data acquisition. The synchrotron X-ray powder diffraction (SXRD) dates were obtained in the MSPD high-resolution diffractometer at the ALBA facility, Barcelona (Spain) with an incident beam with 28 keV energy, λ = 0.4427 Å. High angular resolution mode (MAD set-up) was used on the MSPD-diffractometer. A polycrystalline powder of the same selected composition was contained in a glass capillary. The structure refinements were conducted by the Rietveld method using the FULLPROF refinement program[1]. The line shape of the diffraction peaks was generated using the pseudo-Voigt function. At room

temperature, we refined the scale factor, pseudo-Voigt, zero-point error, the background coefficients corrected for isotropic thermal factors, positional coordinates, and asymmetry parameters. Commercial cell model purchased from Bruker Co. with specific sample stage on a Bruker D8 ADVANCE (Bruker AXS, Germany) with a graphite monochromator (Cu Kα the radiation) were used to carry out the in situ XRD test.

Electrochemical characterization. The powders of active materials were mixed with Ketjen black and polytetrafluoroethylene (PTFE) (70:20:10), loading mass of the whole electrode is 4±0.5 mg/cm^2. Next, the mixture was reeled into a thin film and then using aluminum mesh as the current collector, then dried at 120 °C in a vacuum. Na metal were used as the anode and paired with cathode materials to fabricate 2032 coin-type coin cell, porous glass fibers (Whatman) as the separator, and 1.0 M $NaClO_4$ in ethylene carbonate (EC) /diethyl carbonate (DEC) (1:1 vol) solution with fluorinated ethylene carbonate (FEC) (2%, 5%) as the electrolytes. All cells were assembled in an Ar-filled glove box and then tested at room temperature. The galvanostatic charge/discharge tests used a Neware battery cycler (CT-4008T-5V10mA-164, Shenzhen, China) between 2.0 and 4.0 V. Full cell testing was done by cycling from 0.5 to 2.0 V with NTP as the anode.

Total scattering Experiment

PANalytical Empyrean with Ag source and GaliPIX 3D detector was used to carry out the total scattering experiments. The samples were loaded into Kapton capillary with a

diameter of 0.054 inches and then sealed with epoxy adhesive glue in an argon-full glove box. The diffraction data were then collected in 24 hours from 2 θ of 2° to 140°. The raw powder diffraction data were processed and Fourier transformed to PDF using HighScore plus with a maximum Q value of 18.8 $Å^{-1}$. To reduce the ripple induced by limited maximum Q value the step function was implemented. The real space data was refined by PDFgui[2] and RMCprofile[3]. The instrument parameters were calibrated by refining the structure of a silicon sample.

Reitveld-like "small box" refinements (PDFgui)

The instrument parameters, Q_{broad} and Q_{damp}, are determined by refining the standard silicon powder and then are fixed during the refinement. The refinement procedures are divided into two parts: Firstly the scale factor, lattice parameters, $\delta_2(\sim 1/r^2)$ and isotropy atom displacement parameters are refined and then the refined results are set to the initial values to re-fit the data while the displacement parameters of O and Na are set to anisotropy. Here, $\delta_2(\sim 1/r^2)$ in PDFgui is an empirical parameter for describing the correlated motion.

Supercell-based "big box" modeling (RMCprofile)

First, the 6×6×6 supercell is generated from the unit cell using the lattice parameter obtained from the "small-box" refinement. The generated supercell is shown in Supplementary Fig. 14. The configuration contained a total of 8640 atoms. The real space data G(r) and reciprocal space data F(Q) are refined using a fitting range of 0.2-20 Å and 0.6-18.8 $Å^{-1}$ respectively. The instrument resolution parameters are obtained

from PDFgui refinement. Window distance contraints are used to avoid unphysical structure. The maximum moving of each atom is set to 0.05 Å. To minimize statistical noise, 25 unique RMC configurations were produced and analyzed.

Local correlation coefficients calculation

The local correlation coefficient is defined as

$$P_{ij}(D_{min},D_{max}) = \frac{1}{N_i + N_j}\sum_{k}^{N_i}\frac{1}{N_{shell}}\sum_{l}^{N_j} f(k,l) \quad (1)$$

Where,

$$f(k,l) = \begin{cases} 1, if\ D_{min} \le \left\| \vec{r}_k - \vec{r}_l \right\| \le D_{max} \\ 0, otherwise \end{cases} \quad (2)$$

the inner summation represents the number of atoms of type *j* within a certain shell surrounding the k^{th} atom of type *i*. With such notations, $\sum_{l}^{N_j} \mathrm{f}(k,l)$ denotes the number of atoms of type *j* within a certain shell surrounding the k^{th} atom of type *i*. The normalization factor N_{shell} sums all of the atoms of type-i and type-j contained in the corresponding shell. N_i and N_j then refer to the total number of atoms with type *i* and *j*, respectively.

Density Functional Theory calculation

Density Functional Theory (DFT) calculations were performed with the Vienna Ab-initio Simulation Package (VASP).[4, 5] The interaction between core ion and valence electron were described by the projector augmented wave method (PAW).[6] The exchange correlation was described with spin-polarized generalized gradient

approximations (GGA) in the scheme of Perdew, Burke, Ernzerhof (PBE).[7, 8] An energy cutoff of 500 eV was used with the Monkhorst k-points[9] sampling scheme (4×4×4 for geometry optimization, while a larger grid of 8×8×8 was used for energy computation). The conjugated gradient method was used for geometry optimization, and all atomic coordinates were fully relaxed until the maximal force on each atom was less than 0.02 eV $Å^{-1}$, with the convergence condition for energy being 10^{-4} eV. Considering the strong correlation effect of transition metal, Hubbard U correction (GGA+U) was used in this work. An effective Hubbard U of 3.9, 3.52, and 5.5 eV was adopted for the *d* orbit of Fe, Co, and Ni, respectively.[10] The Na^+ migration pathway and corresponding energy barrier were optimized with the nudged elastic band (NEB) method.[11]

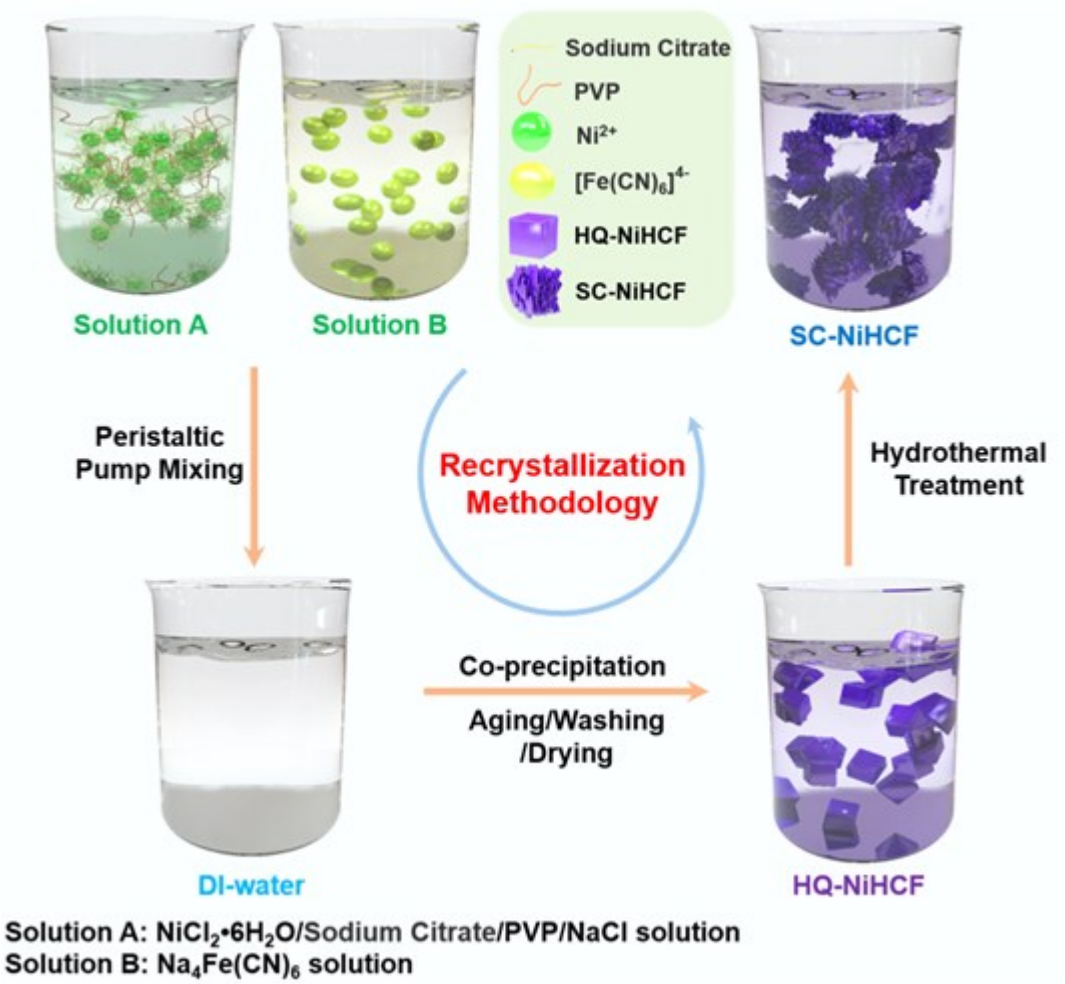

Supplementary Fig. 1. Schematic illustration showing the synthesis process of SC-NiHCF. Here high-quality nickel hexacyanoferrate were marked as HQ-NiHCF, the samples after hydrothermal treatment were labeled as SC-NiHCF.

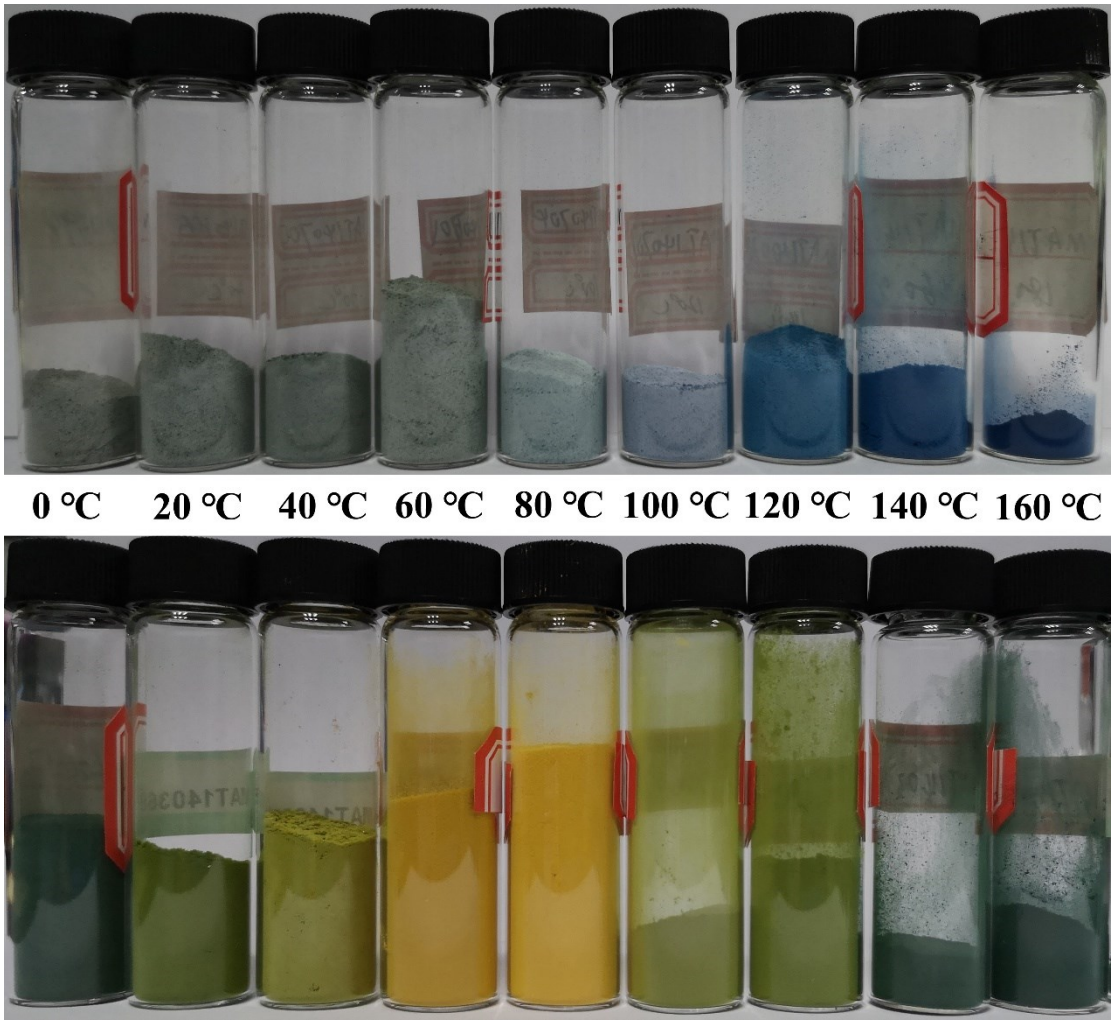

Supplementary Fig. 2. Digital photos of the as-prepared PBAs. Nickel-based Prussian blue analogues (up) and cobalt-based Prussian blue analogues (down) that prepared under the different temperature from 0 to 160 degree, respectively.

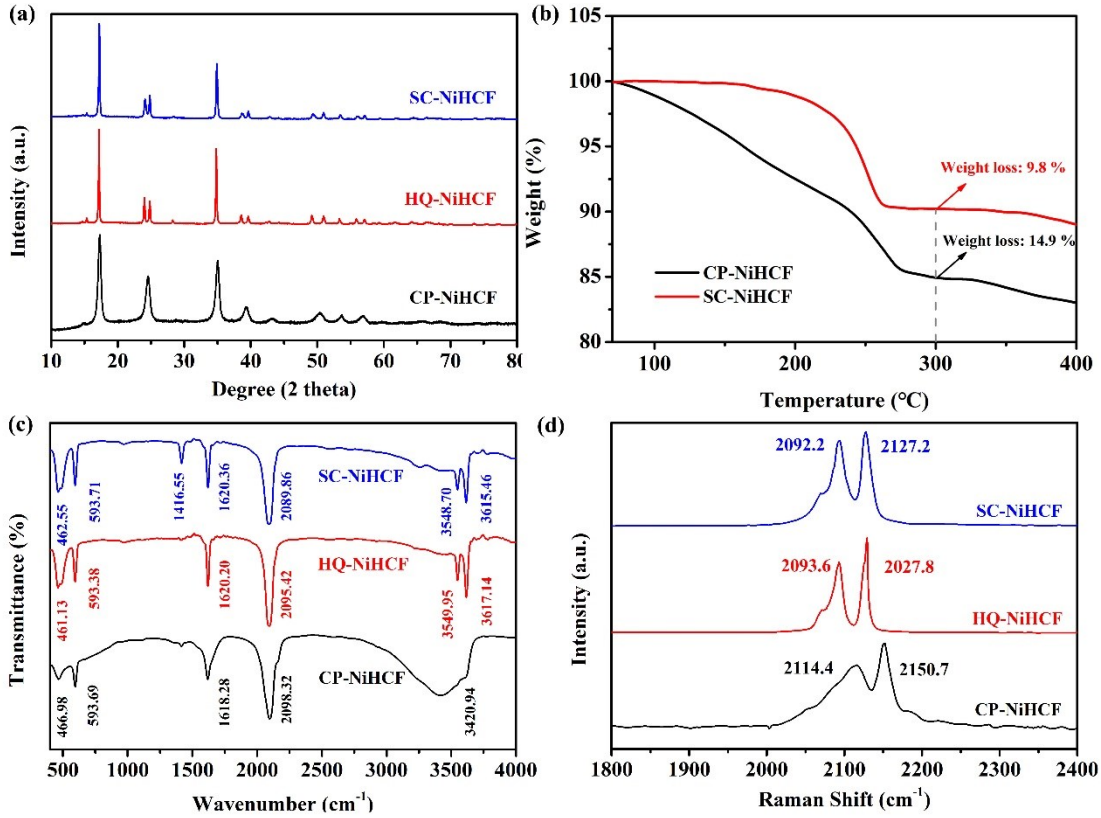

Supplementary Fig. 3. Physical characterization of the nickel-based Prussian blue analogues. **a,** XRD. **b,** TG. **c,** FTIR. **d,** Raman

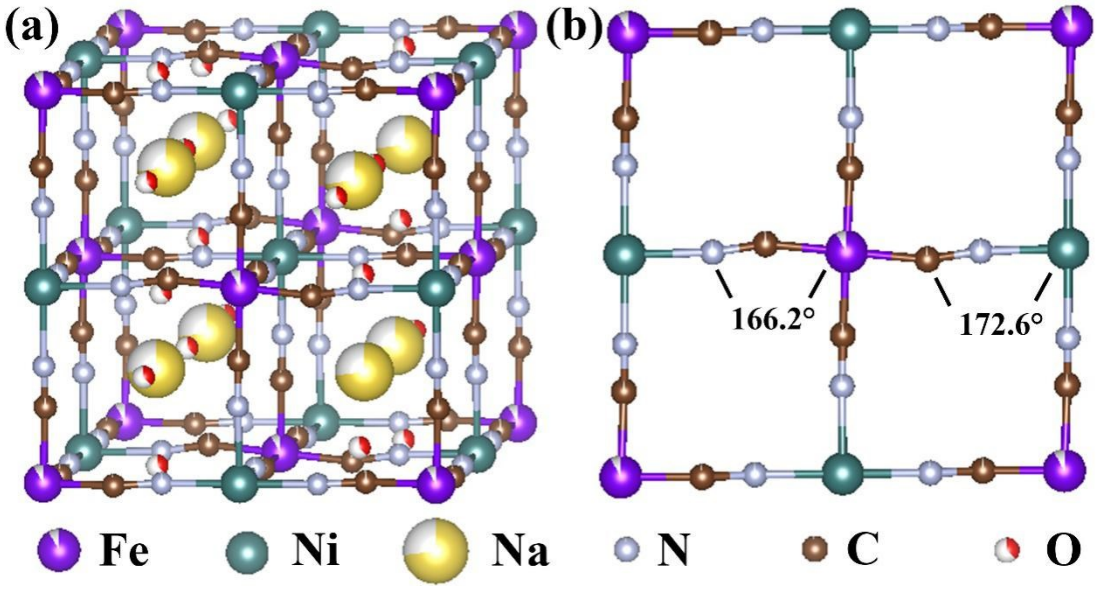

Supplementary Fig. 4. Refined structure model of the SC-NiHCF from the structure refinement of neutron diffraction**.**

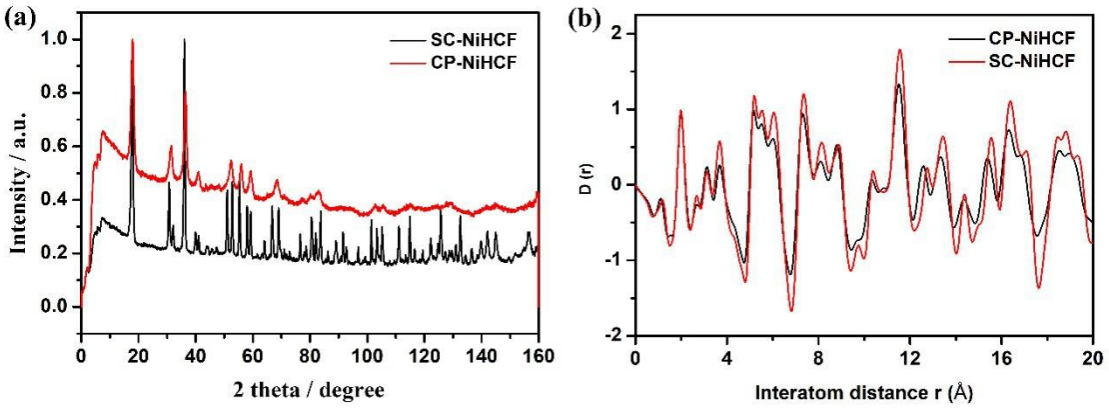

Supplementary Fig. 5. The comparison of CP-PBA and SC-PBA. **a,** Neutron powder diffraction pattern of CP-NiHCF (red line) and SC-NiHCF (black line). **b,** Pair distribution function, D(r),of CP-NiHCF (black line) and SC-NiHCF (red line). The consistency at positions of peaks below 10 Angstrom indicates the two have similar local structure but with varying defect content. However, as the interatom distance increases, the peaks of SC-PBA shift to high-r region, which means discrepancy of arrangement of unit cell.

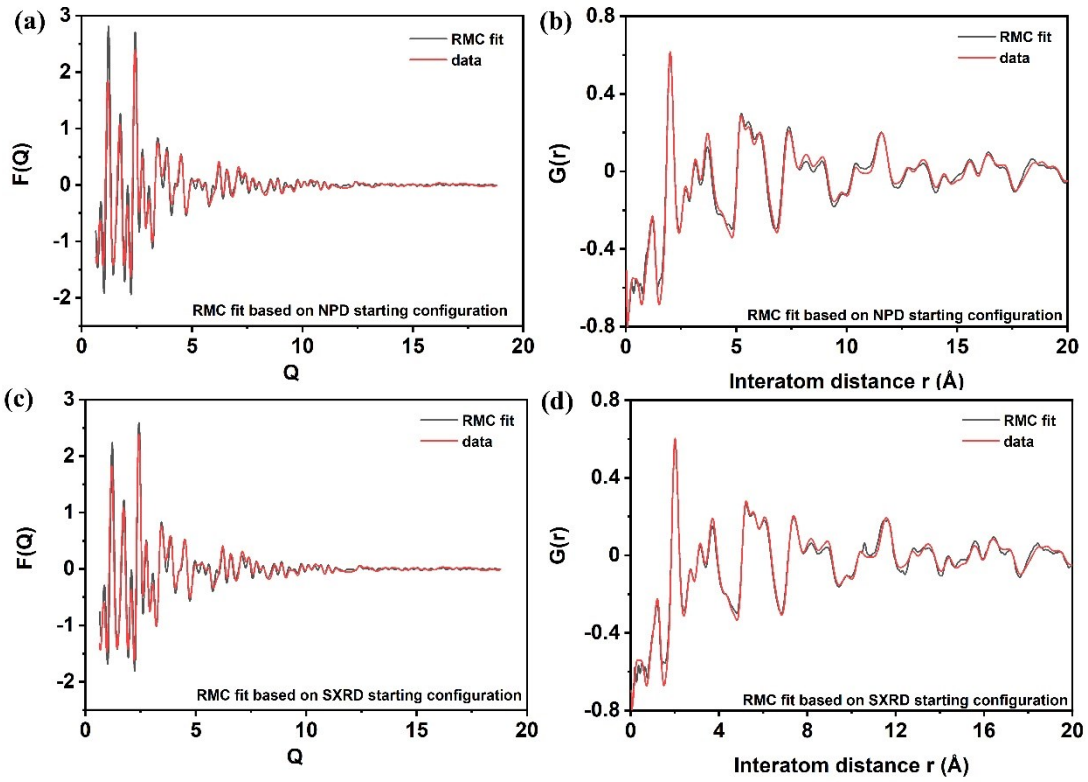

Supplementary Fig. 6. The comparison based on different starting configuration of RMC method. **a,b** show the refinement of reciprocal space and real space data using the NPD Reitveld result as starting configuration while **c,d** shows the refinements using SXRD Reitveld result as starting configuration.

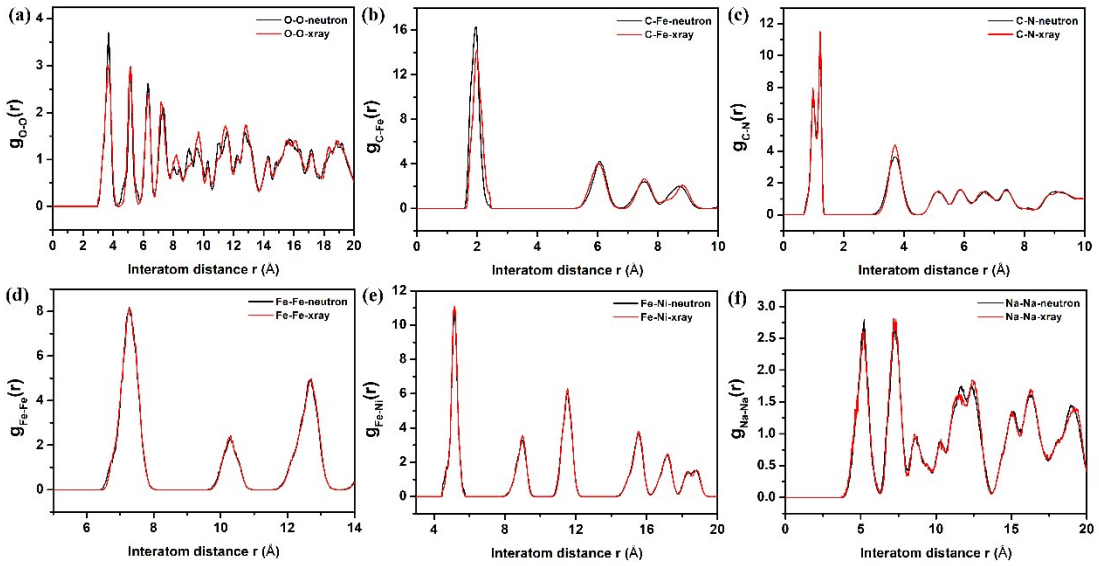

Supplementary Fig. 7. The comparison of partial pair correlation function obtained from different starting model.

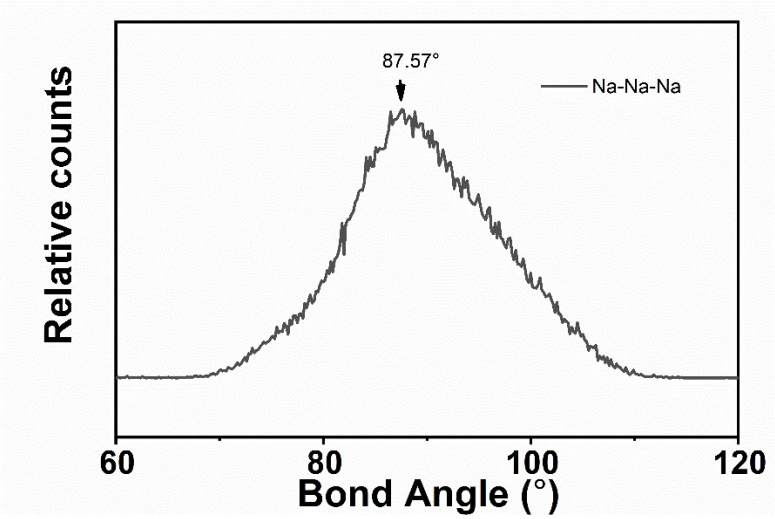

Supplementary Fig. 8. Bond angle distribution of Na-Na-Na based on RMC simulation.

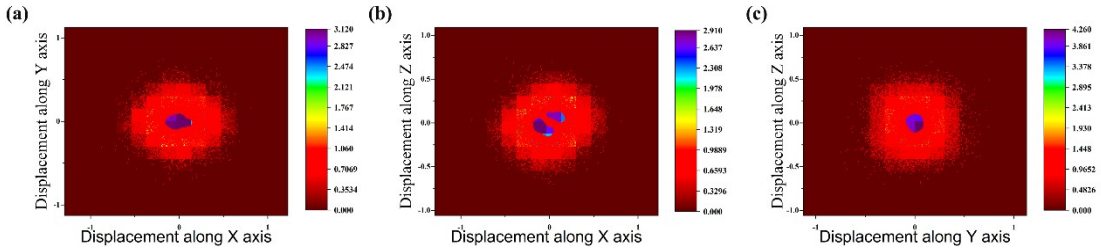

Supplementary Fig. 9. The kernel density plot of displacement analysis of Na ion along **a** X-Y plane; **b** X-Z plane; **c** Y-Z plane.

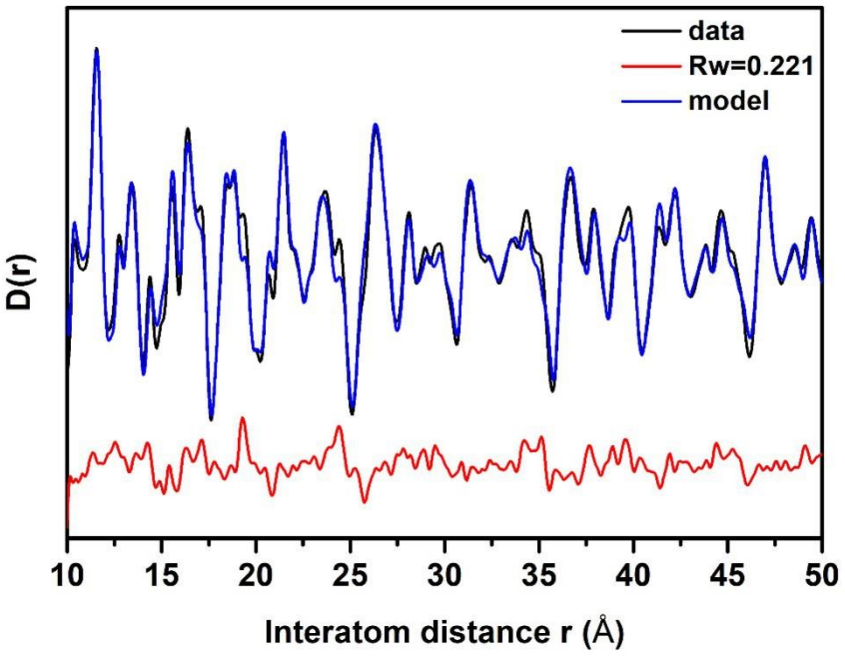

Supplementary Fig. 10. PDFgui refinement patterns ranging from 10-50 Å.

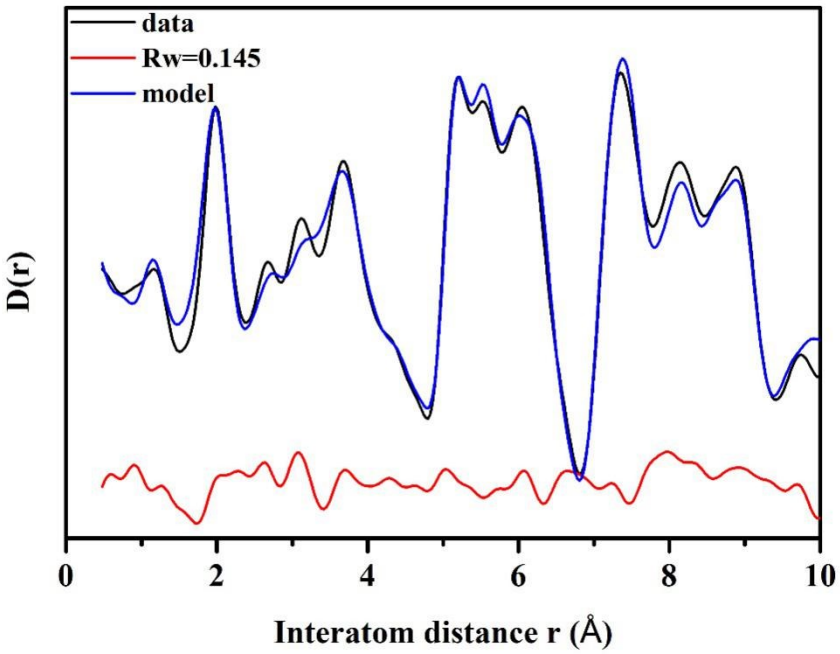

Supplementary Fig. 11. PDFgui refinement patterns ranging from 0.5-10 Å.

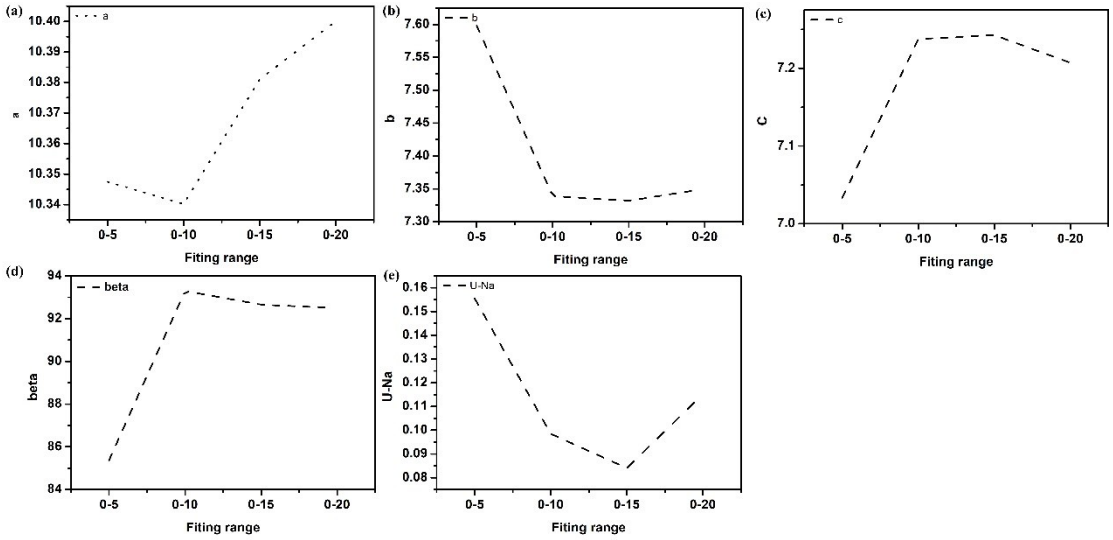

Supplementary Fig. 12. The values of lattice parameters of a, b, c, beta-angle and the atom displacement parameter of sodium obtained from refinement under different fitting range. Those values vary as the fitting range changes which indicates the local structure inhomogeneity.

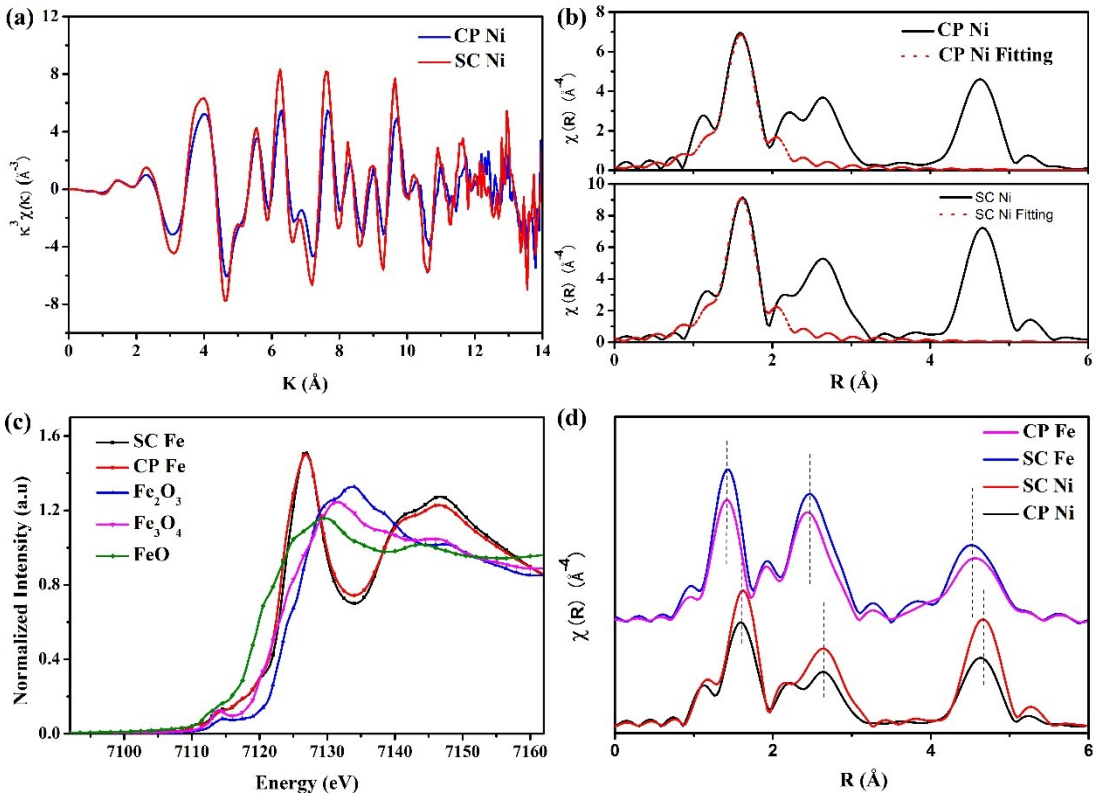

Supplementary Fig. 13. EXAFS data analysis. **a,** The total Ni K-edge EXAFS spectrum with k^3-weight in k-space for CP-NiHCF and SC-NiHCF. **b,** Fourier transform of the EXAFS spectrum and the corresponding fitting curve for CP-NiHCF and SC-NiHCF in Ni K-edge. **c,** Fe K-edge XANES spectra of CP-NiHCF, SC-NiHCF, Fe_2O_3, Fe_3O_4, and FeO reference. **d,** Fourier transform of the EXAFS spectrum both in Fe K-edge and Ni K-edge for CP-NiHCF and SC-NiHCF.

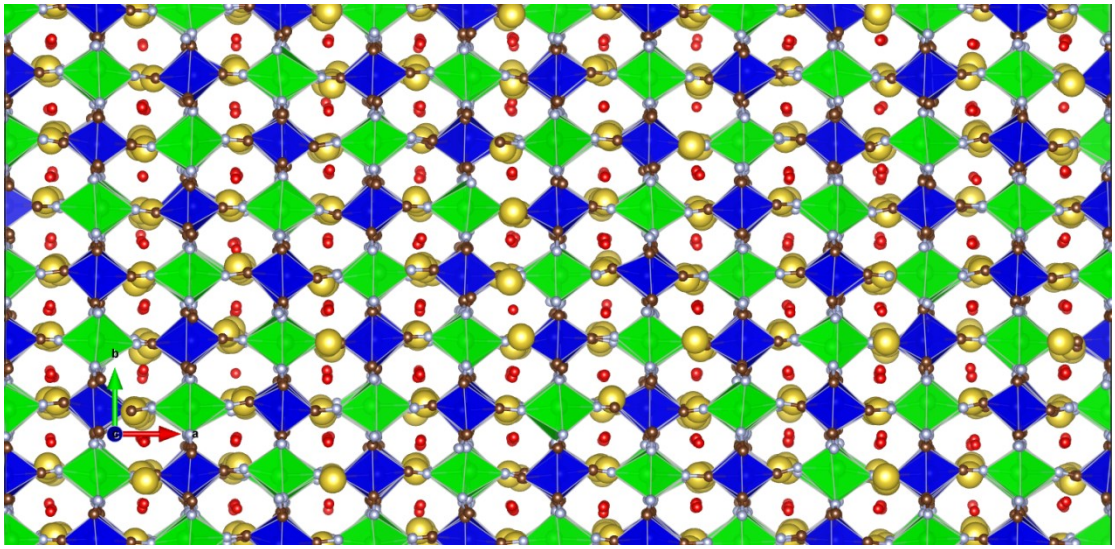

Supplementary Fig. 14. The polyhedral view of the super cell that applied in the RMC simulation.

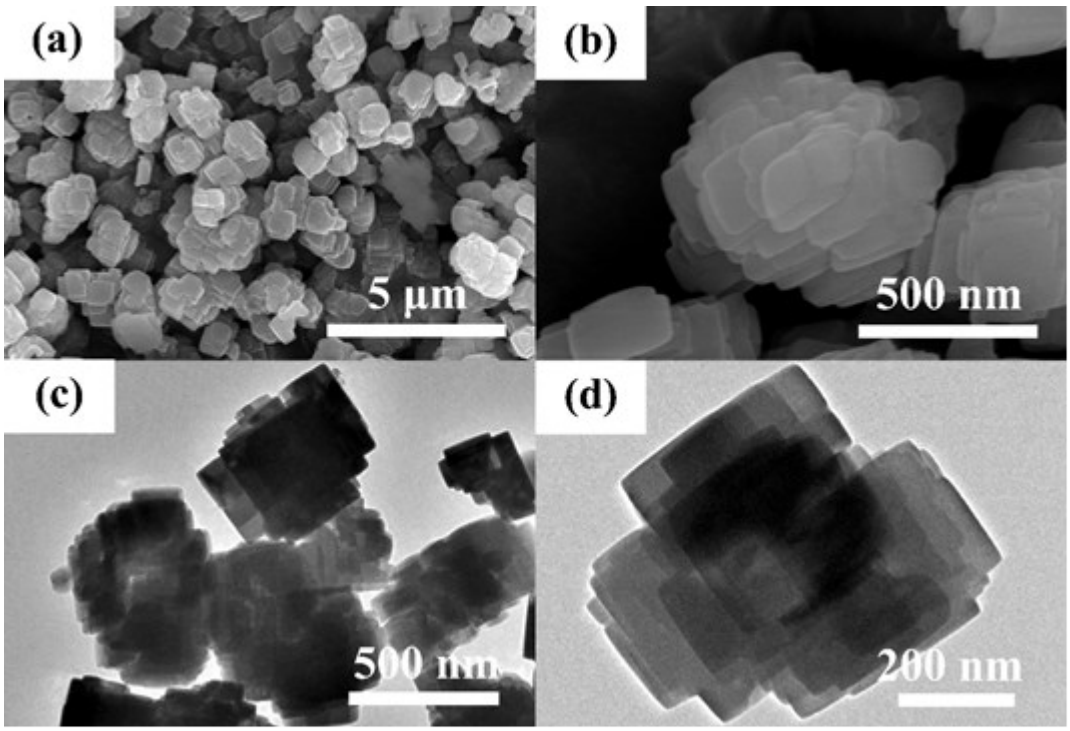

Supplementary Fig. 15. The morphology of the SC-NiHCF hierarchical particles. **a, b,** SEM of the SC-NiHCF with scale bar of 5 um and 500 nm, respectively. **c, d,** TEM figures of the SC-NiHCF.

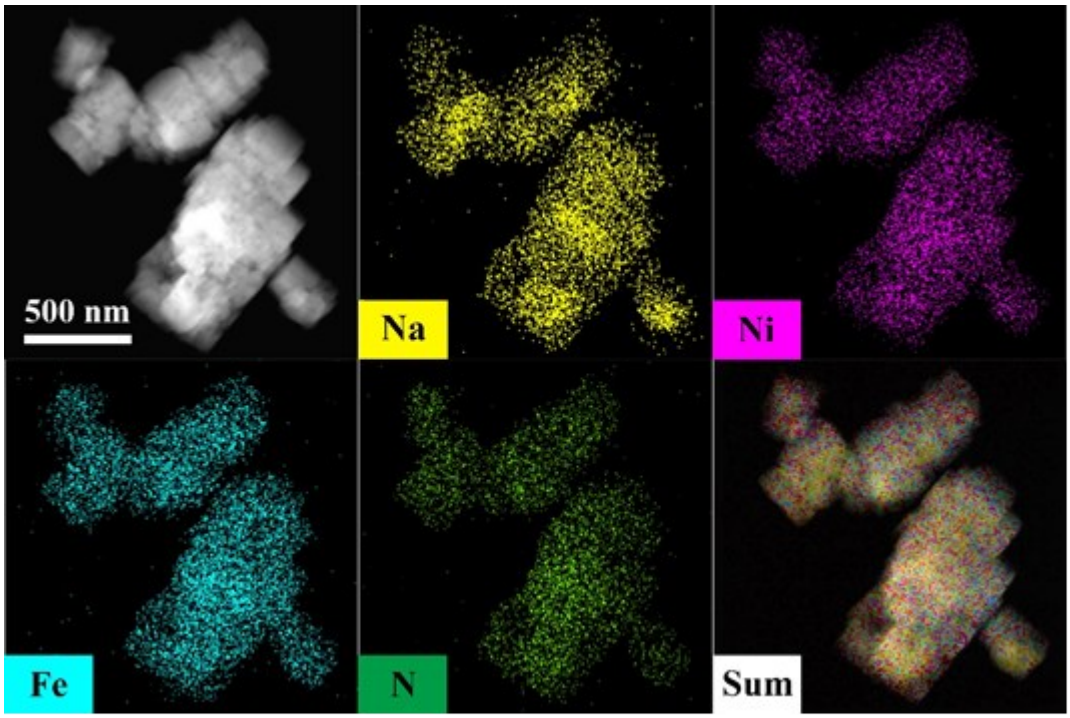

Supplementary Fig. 16. TEM energy dispersive spectroscopy (EDS) images mapping of SC-NiHCF.

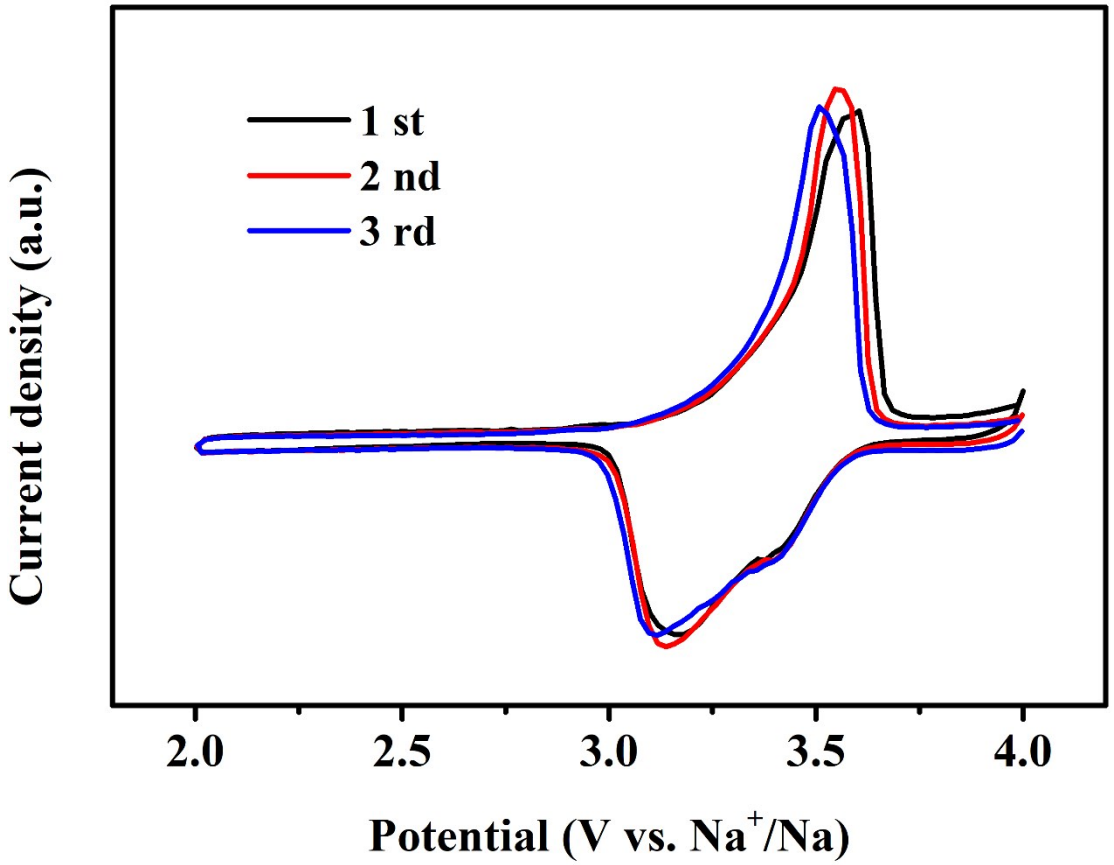

Supplementary Fig. 17. The first 3 cycles charge and discharge galvanostatic curves of the SC-NiHCF.

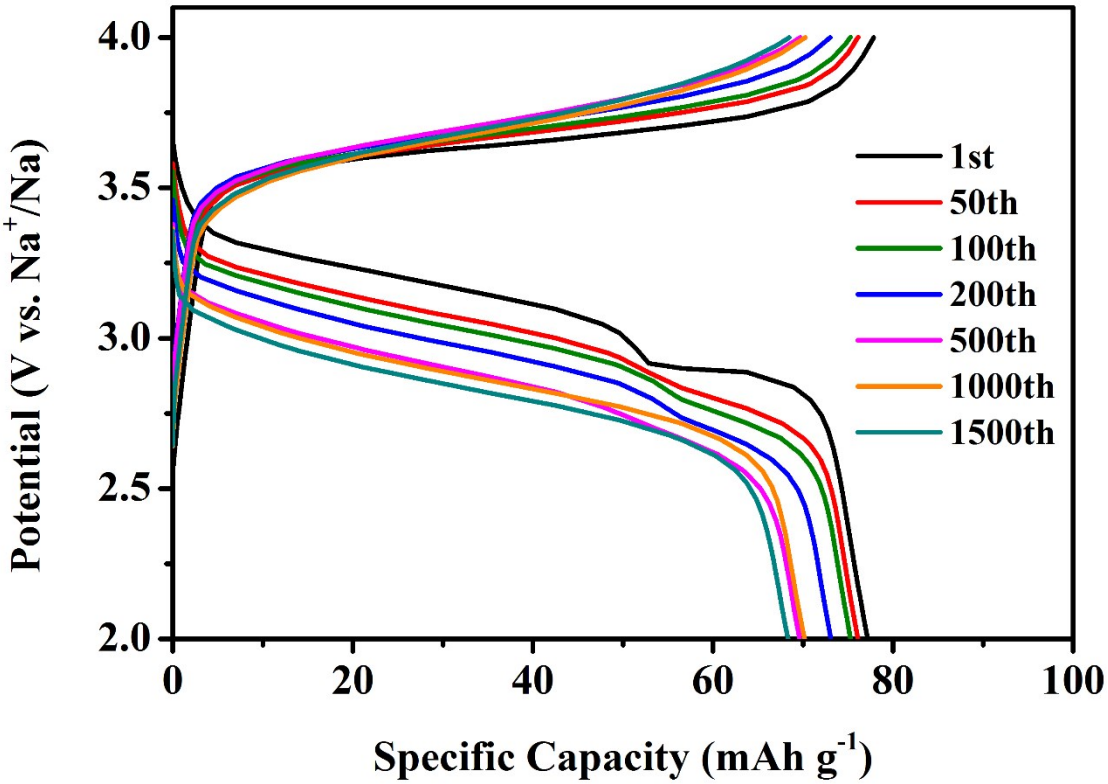

Supplementary Fig. 18. The charge and discharge curves of the SC-NiHCF in the 1M $NaClO_4$ EC/DEC (1:1) with 5% FEC electrolyte.

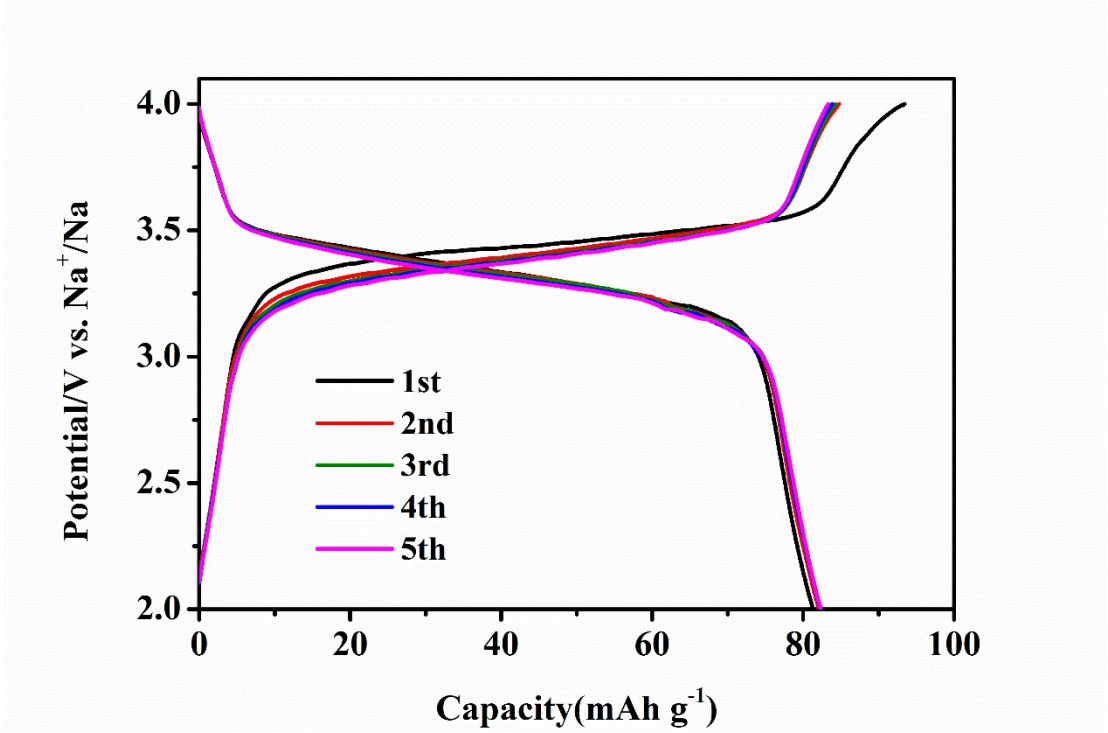

Supplementary Fig. 19. First 5 cycles of SC-NiHCF at current density of 0.1 C.

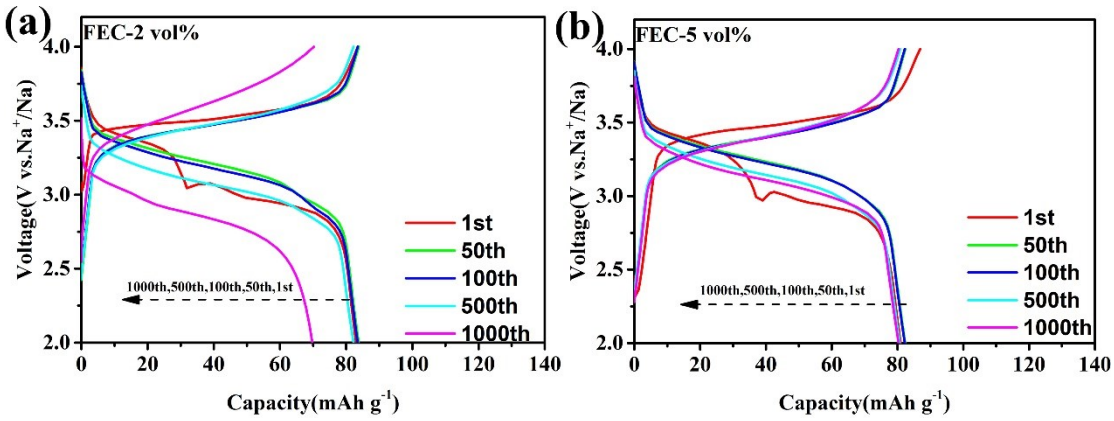

Supplementary Fig. 20. The charge and discharge curves of SC-NiHCF in the electrolytes with the different amount of FEC additions. **a, 2**% of FEC. **b**, 5% of FEC.

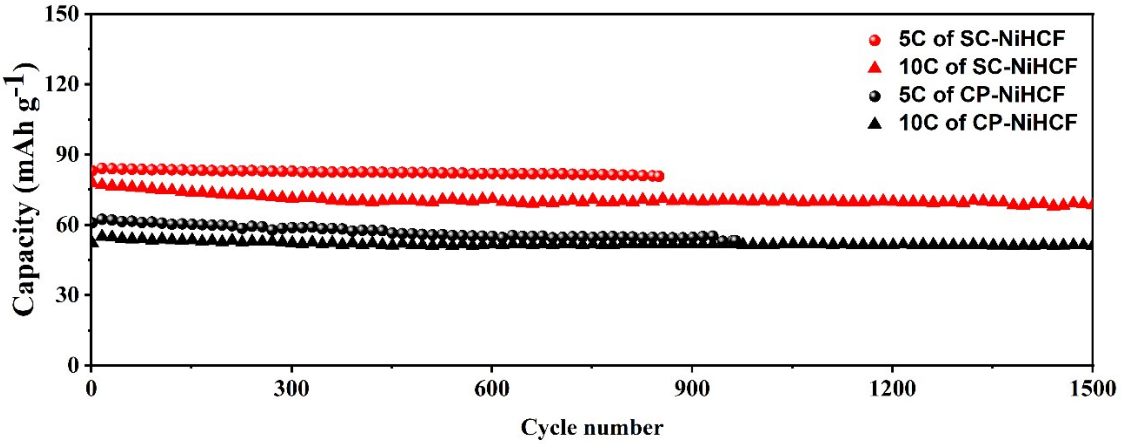

Supplementary Fig. 21. The cycling stability of CP-NiHCF and SC-NiHCF at the current density of 5C and 10C, respectively.

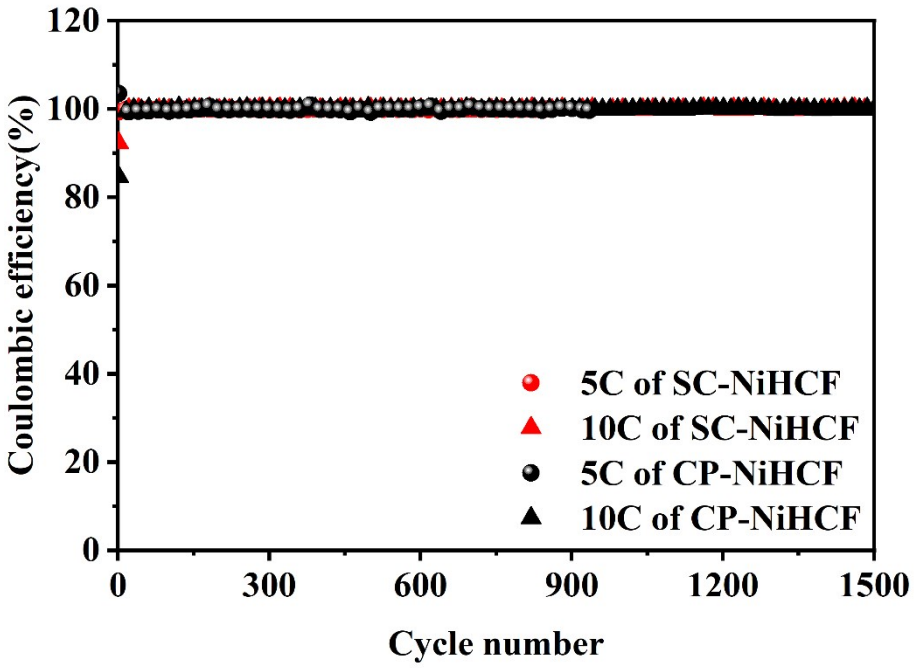

Supplementary Fig.22. The charge and discharge coulombic efficiency of the CP-NiHCF and SC-NiHCF.

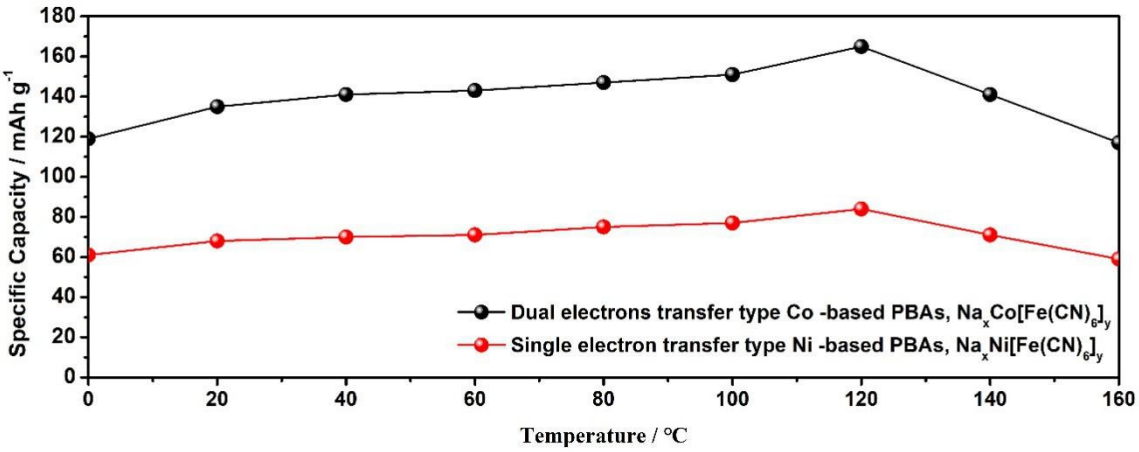

Supplementary Fig. 23. The first cycle discharge capacity of typical dual electrons transfer type Co-based PBAs and single electrons transfer type Ni-based PBAs synthesized under the different temperature.

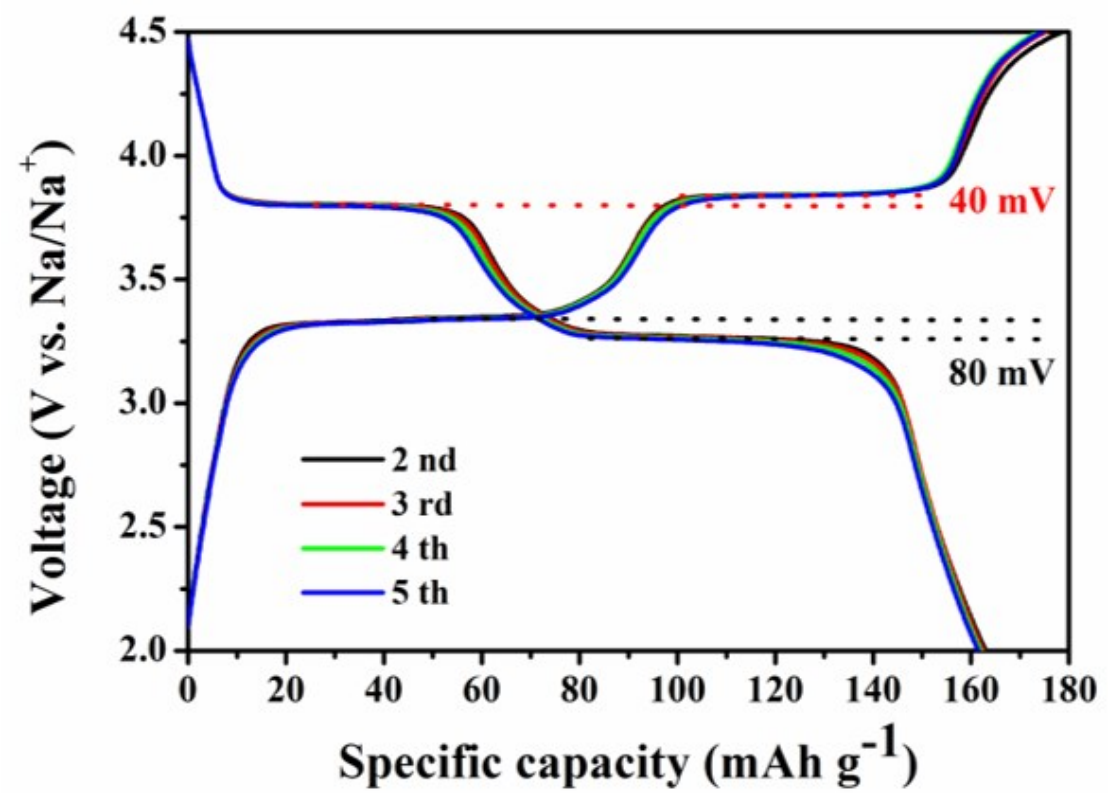

Supplementary Fig. 24. Charge and discharge curve of $Na_2CoFe(CN)_6$ synthesized by the secondary crystallization method at 0.1C at 2-4.5 V.

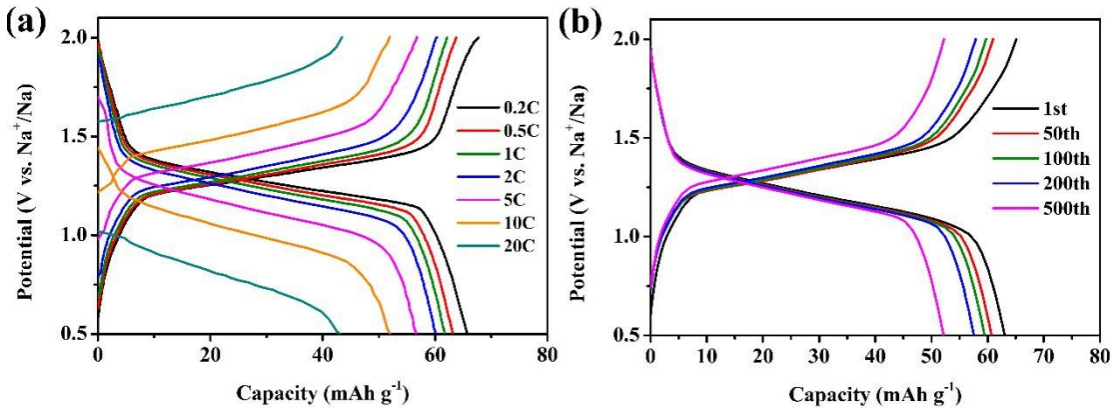

Supplementary Fig. 25. Charge and discharge curve of SC-NiHCF/NTP full cell. **a,** The full-cell charge and discharge curves at the various rate (1C= 80 mA g^{-1}). **b,** Charge and discharge curves of the full-cell at the various cycles.

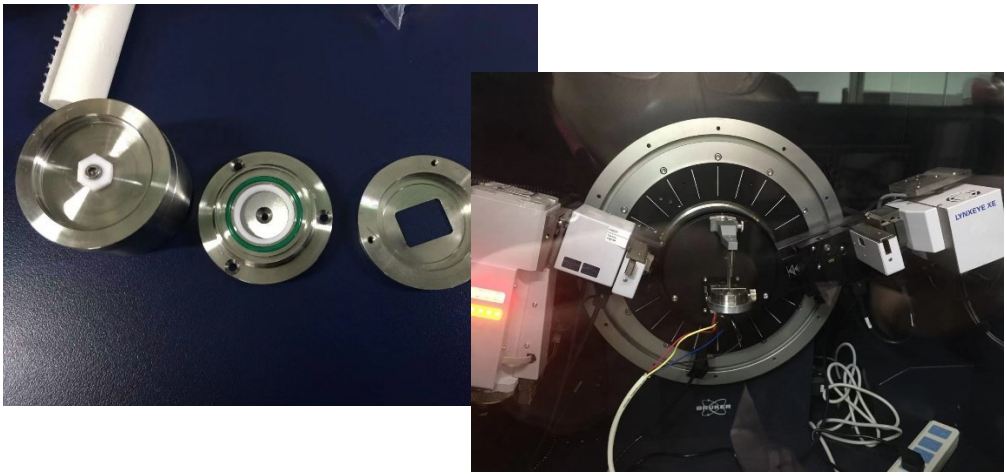

Supplementary Fig. 26. The photograph of the in situ XRD test facilities.

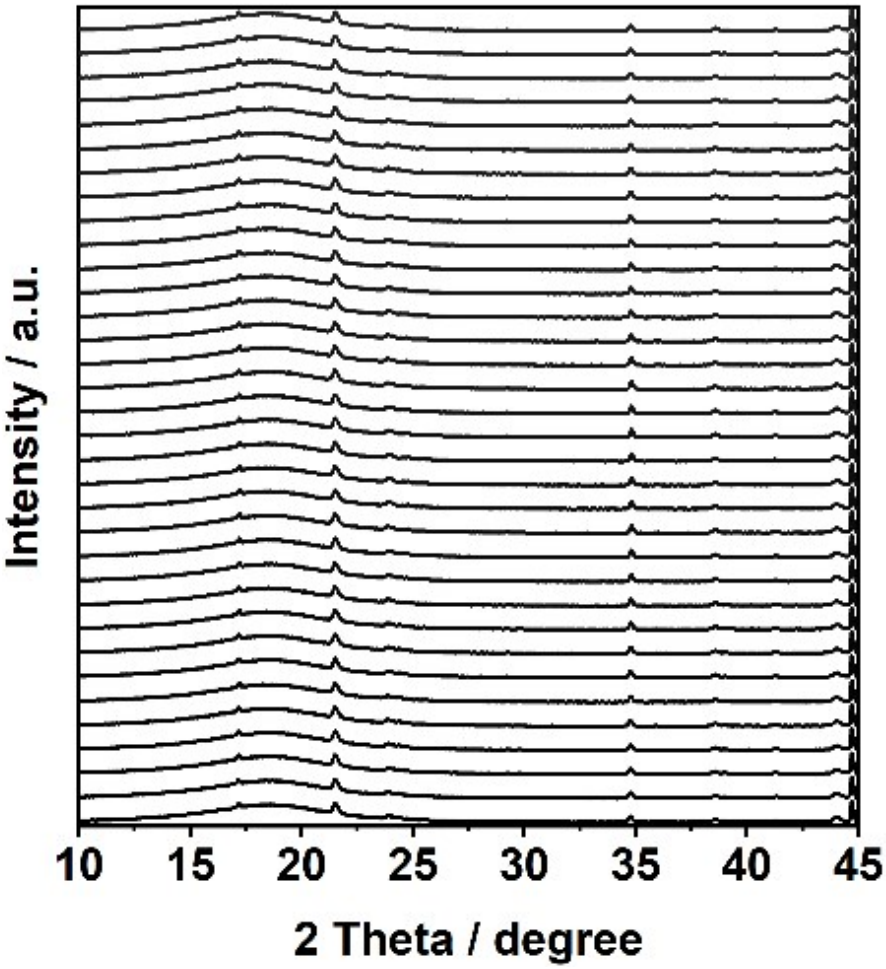

Supplementary Fig. 27. The in situ XRD pattern of a single cycle.

S.G. P21/n a = 10.3043(5) Å b = 7.4024(3) Å c = 7.1707(3)Å α = 90° β = 92.5010(5)° γ = 90°						
Atom	Wyck.	*x/a*	*y/b*	*z/c*	occ	Uiso
N1	4 e	0.0048	0.1984	0.197	0.97	0.026
N2	4 e	0.3022	0.504	0.5022	0.97	0.017
N3	4 e	0.0030	0.8063	0.209	0.97	0.020
C1	4 e	0.005	0.303	0.323	0.97	0.031
C2	4 e	0.183	0.517	0.523	0.97	0.031
C3	4 e	0.0034	0.6838	0.2989	0.97	0.004
Fe	2 d	0.000	0.500	0.500	0.97	0.001
Ni	2 a	0.000	0.000	0.000	1	0.013
Na	4 e	0.238	0.522	0.011	0.738	0.063
O	4 e	0.243	0.281	0.263	0.379	0.037
O2	4 e	0.251	0.205	0.689	0.379	0.048

Supplementary Table 1 Atomic coordinates for the SC-NiHCF obtained from the structure refinement of neutron diffraction.

Chemical formula	Test methods
$Na_{1.64}Ni[Fe(CN)_6]_{0.92}$•1.83 H_2O	Inductively coupled plasma optical emission spectrometer (ICP-OES)+ Thermogravimetric analysis (TGA)
$Na_{1.48}Ni[Fe(CN)]_{0.97}$•1.56$H_2O$	Neutron diffraction (ND)

Supplementary Table 2 The chemical formula of the SC-NiHCF obtained by three kinds of test methods.

Sample name	Na	Fe	Ni
CP-NiHCF	4.24%	9.68%	13.72%
HQ-NiHCF	10.91%	13.86%	16.70%
SC-NiHCF	11.82%	15.10%	17.13%

Supplementary Table 3 ICP-OES anylasis of CP-NiHCF, HQ-NiHCF and SC-NiHCF.

Sample name	Chemical formula
CP-NiHCF	$Na_{0.79}Ni[Fe(CN)_6]_{0.74}$
HQ-NiHCF	$Na_{1.67}Ni[Fe(CN)_6]_{0.87}$
SC-NiHCF	$Na_{1.76}Ni[Fe(CN)_6]_{0.93}$

Supplementary Table 4 The chemical formula of the prepared samples. By ICP calibration of Na, Ni, Fe contents, the composition of the CP-NiHCF, HQ-NiHCF and SC-NiHCF can be determined as $Na_{0.79}Ni[Fe(CN)_6]_{0.74}$, $Na_{1.67}Ni[Fe(CN)_6]_{0.87}$, $Na_{1.76}Ni[Fe(CN)_6]_{0.93}$.

Fitting range (Å)	a(Å)	b (Å)	c (Å)	β (°)	Uiso-Na	Rw
0.5-5	10.34(0.7)	7.60(1.4)	7.03(1.5)	85.37(4.5)	0.16(0.29)	0.145
0.5-10	10.34(0.23)	7.34(0.13)	7.24(0.15)	93.298(1.1)	0.099(0.05)	0.152
0.5-15	10.38(0.16)	7.33(0.07)	7.24(0.086)	92.65(0.69)	0.084(0.03)	0.173
0.5-20	10.40(0.1)	7.35(0.05)	7.21(0.07)	92.50(0.55)	0.12(0.036)	0.183

Supplementary Table 5 The refined parameter of SC-NiHCF with different range using isotropic atom displacement parameter of Na.

Fitting range (Å)	A (Å)	b (Å)	c (Å)	β (°)	Uiso-N	Uiso-C	Uiso-Fe
0.5-10	10.329(0.25)	7.346(0.16)	7.242(0.15)	93.216(1.4)	0.04305(0.061)	0.0111(0.014)	0.00573(0.011)

Fitting range (Å)	Uiso-Ni	U11-Na	U22-Na	U33-Na	U11-O	U22-O	U33-O
0.5-10	0.0155(0.013)	0.1714(0.53)	0.0623(0.38)	0.0736(0.48)	0..000136 (0.049)	0.0806(0.2)	0.0497(0.19)

Supplementary Table 6 PDFgui refined parameters of SC-NiHCF with fitting range of 0.5-10 Angstrom using anisotropic atom displacement parameter of Na.

Characterize method	Ni-N distance (Å)
EXAFS	2.050
PDF	2.080
	2.036
NPD	2.073
	2.039

Supplementary Table 7 The atomic distance between Ni and N obtained by different methods.

Sites	8c	24d (1-2)		32f (1-3)		
Vs-Perfect (V)	2.81	3.28		3.12		3.03
Vs-Defect (V)	2.38	3.03	1.01	2.84	2.48	2.23

Supplementary Table 8 Relative sodiation potential of $Na_xNi[Fe(CN)_6]$ with Na^+ occupying different cation interstitial sites.

References

1. J. Rodríguez-Carvajal, Physica B: Condensed Matter, 1993, **192**, 55.
2. C. L. Farrow, P. Juhas, J. W. Liu, D. Bryndin, E. S. Božin, J. Bloch, T. Proffen and S. J. L. Billinge, J. Phys.: Condens. Matter, 2007, **19**, 335219.
3. H. Y. Playford, L. R. Owen, I. Levin and M. G. Tucker, Annu. Rev. Mater. Res., 2014, **44**, 429.
4. G. Kresse and J. Hafner, Phys. Rev. B, 1994, **49**, 14251.
5. G. Kresse and J. Furthmüller, Phys. Rev. B, 1996, **54**, 11169.
6. P. E. Blöchl, Phys. Rev. B, 1994, **50**, 17953.
7. J. P. Perdew, K. Burke and M. Ernzerhof, Phys. Rev. lett., 1996, **77**, 3865.
8. W. Kohn and L. J. Sham, Phys. Rev., 1965, **140**, A1133.
9. H. J. Monkhorst and J. D. Pack, Phys. Rev. B, 1976, **13**, 5188.
10. Y. You, H. R. Yao, S. Xin, Y. X. Yin, T. T. Zuo, C. P. Yang, Y. G. Guo, Y. Cui, L. J. Wan and J. B. Goodenough, Adv Mater, 2016, **28**, 7243.
11. G. Henkelman, B. P. Uberuaga and H. Jónsson, J. Chem. Phys., 2000, **113**, 9901.